RSC Advances

ROYAL SOCIETY OF CHEMISTRY

www.rsc.org/advances

Journal Name

ARTICLE

Crucial role of sustainable liquid junction potential for solar-to-carbon monoxide conversion by photovoltaic photoelectrochemical system

Received 00th January 20xx,
Accepted 00th January 20xx

DOI: 10.1039/x0xx00000x

www.rsc.org/

Yoshitsune Sugano,[a] Akihiko Ono,[a] Ryota Kitagawa,[a] Jun Tamura,[a] Masakazu Yamagiwa,[a] Yuki Kudo,[a] Eishi Tsutsumi,[a] Satoshi Mikoshiba[a]

Solar energy conversion to carbon monoxide (CO) is carried out using a wired photovoltaic photoelectrochemical (PV PEC) system under simulated solar light irradiation. The PV PEC system promotes CO generation from carbon dioxide and water with approximately 2.0% solar-to-CO conversion efficiency (η_{CO}) for 2 h. This is achieved via contributions from electrolyte conditions, which generate a sustainable liquid junction potential, in addition to the combination of efficient visible light absorption by a triple-junction amorphous silicon PV cell with high electrode activities with low overpotentials. Estimations of energy conversion efficiency based on the electrochemical properties of the PV cell and electrodes exhibit that liquid junction potential makes a huge contribution for η_{CO}. Moreover, the liquid junction potential created by bubbling two kinds of carrier gases produces sustainable chemical bias. This system may contribute to new strategies for the development of sustainable artificial photosynthesis.

1. Introduction

Artificial photosynthesis has attracted much attention as a green technology for addressing environmental problems such as global warming and energy issues.[1] Some components of artificial photosynthesis technologies such as light-harvesting,[2] water splitting,[3] hydrogen (H_2) production,[4] and carbon dioxide (CO_2) reduction[5] have been reported, and the suitable materials such as electrodes, photocatalysts with metal/metal oxide co-catalysts, and organometallic complexes have been researched for these technologies. Recently, researchers have proposed fuel production from water and CO_2 by artificial photosynthesis.[6]

Photovoltaic (PV) cells are one of the photoelectric conversion elements that enable excitation by visible light irradiation. Among them, triple-junction amorphous silicon (3jn-a-Si) PV cells, which are inexpensive and have a trilaminar structure of amorphous silicon and silicon-germanium alloy, possess wide visible light absorption ranges and a high open circuit voltage (V_{OC}, 2.1 V). Reece et al. reported that the 3jn-a-Si PV cell with cobalt (Co)-based and alloy metal catalysts promotes solar-driven water (H_2O) splitting with high conversion efficiency (approximately 4.7%).[7] This is because in addition to the above-mentioned 3jn-a-Si PV cell properties, the Co-based anode catalyst and alloy metal cathode catalyst efficiently decrease partial overpotentials for H_2O oxidation and H_2 production, respectively. However, adaptation of artificial photosynthesis-PV photoelectrochemical (PEC) systems to CO_2 reduction may be difficult due to the larger overpotential for CO_2 reduction.[8] Therefore, more suitable cathode catalysts with low overpotential for CO_2 reduction are required. Recently, it has been reported that a gold (Au) nanoparticle electrode, synthesized by a pulse-oxidation process, promotes efficient CO_2 reduction to produce carbon monoxide (CO) with a lower overpotential.[9] In addition, most recently a solar fuel device using copper indium gallium selenide (CIGS)-based PV with Co_3O_4 anode and Au nanoparticle cathode promoted high conversion efficiency for CO production.[6h] However, research of the electrolyte for efficient and sustainable solar fuel systems for CO_2 reduction has been scarce.

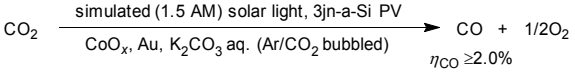

Scheme 1 The PV PEC system for CO production using a wired PV cell with CoO_x and Au nanoparticle electrodes in different carbonate electrolytes.

Herein, we report that a wired 3jn-a-Si PV PEC system with cobalt oxide (CoO_x) and Au nanoparticle electrodes in different carbonate electrolytes promotes solar energy conversion from CO_2 to CO with H_2O as an electron source (Scheme 1). For pursuing a feasible technology, we selected a 3jn-a-Si PV cell as a photoelectric conversion element because they supply enough voltage to progress this system. Moreover, their low manufacturing energy may contribute to obtaining high energy

[a] Corporate Research & Development Center, Toshiba Corporation, Kawasaki, 212-8582, Japan.
E-mail: yoshitsune.sugano@toshiba.co.jp; Fax: +81-44-520-1307
† Electronic Supplementary Information (ESI) available. See
DOI: 10.1039/x0xx00000x

return on investment in a practical system. The solar-to-CO conversion efficiency (η_{CO}) of the system is approximately 2.0% for 2 h. The η_{CO} value is achieved largely by the contribution of a sustainable liquid junction potential. Continuously bubbling different gases (CO_2/Ar) through the carbonate electrolytes generates a difference of pH and produces a liquid junction potential, which decreases the overpotential in the actual operating potential and enhances the η_{CO} value. In addition, the theoretical estimation of η_{CO} based on the electrochemical measurements supported the significance of the liquid junction potential.

2. Experimental section

2.1. Materials

A 3jn-a-Si PV cell was purchased from Xunlight Corporation. A gold plate (thickness 0.1 mm, 99.99%) was purchased from Sigma-Aldrich. Potassium carbonate (K_2CO_3, 99.5%) was purchased from Wako Pure chemical Industries, Ltd. Sulfuric acid (H_2SO_4, 96%) was purchased from Kanto Chemical Corporation, Inc. SELEMION™ (DSV) anion exchange membrane was purchased from AGE Engineering Co. Ltd.

2.2. Preparation of CoO_x anode

The anode was directly prepared on the photosensitive surface of 3jn-a-Si PV cells by the reactive sputtering method (apparatus: type SRV-4300 manufactured by Shinko-Seiki Co., Ltd), which were performed at Kyodo International, Inc. The target was Cobalt, and a mixture of 30% O_2/(O_2 + Ar) was used as the sputtering gas (1.0 Pa). RF power was 150 W, and the operating temperature was 453 K. A CoO_x layer thickness of about 15 nm was achieved by controlling the deposition time.

2.3. Preparation of Au nanoparticle cathode

The cathode was prepared by the pulse-oxidation process as follows: A gold plate was annealed at 1023 K (3 K min^{-1}) for 12 h under air flow, and etched in fresh aqua regia for 20 s. An Au plate electrode (1 cm^2) masked by epoxy resin was pulse-oxidized at 0.0 to +2.0 V *vs.* Hg/Hg_2SO_4 (sat'd K_2SO_4) (symmetric 1 kHz square-wave pulse) in a sulfuric acid solution (0.5 M) for 2 h using a cell test system (Solartron Analytical, 1470E). Finally, the pulse-oxidized Au electrode was electrically reduced at −0.40 V *vs.* Reversible Hydrogen Electrode (RHE) until the reductive current was stabilized.

2.4. Reaction procedure

Electrochemical measurement of CoO_x anode: The tafel plots were measured by the following method: An indium tin oxide (ITO)/Si electrode coated with CoO_x by the reactive sputtering method similar to PV coated with CoO_x was used as the anode electrode. A platinum mesh was used as a counter electrode. The electrolyte was K_2CO_3 solution (0.25 M) with saturated CO_2 (pH <7.3), or Ar/CO_2 bubbled through the anolyte (pH 9.2) and catholyte (pH <7.3). The potential was applied by potentiostatic method (0.90 V to 1.50 V *vs.* Ag/AgCl (3M NaCl); step size: 50 mV; step time: 300 s) and the applied potential was measured by a Ag/AgCl reference electrode (3M NaCl).

Electrochemical measurement of Au nanoparticle cathode: Before use in the Tafel plots measurement, the Au nanoparticle electrode was pre-refreshed by cyclic voltammetry (−1.30 V to +1.40 V *vs.* Ag/AgCl (sat'd KCl); 150 mV s^{-1}; 50 cycle) in K_2CO_3 solution (0.25 M) with saturated CO_2 (pH <7.3). A platinum mesh was used as counter electrode. The electrolyte was K_2CO_3 solution (0.25 M) with saturated CO_2 (pH <7.3). The applied potential was measured by a Ag/AgCl reference electrode (sat'd KCl). The current density and faraday efficiencies of products at various applied potentials were measured at 2 h after potential application. In addition, the gas-phase products were analyzed by a 7890A gaschrograph (Agilent GC System; Column: GS-GASPRO 30 m × 0.320 mm). The liquid-phase products were analyzed by an ion chromatograph (Waters IC System; 2695 Separation Module equipped with Waters 432 Conductivity Detector; Column: Thermo Dionex™ IonPac™ AS11 4 mm × 250 mm and AG11 4 mm × 50 mm).

PV PEC system for CO production: Before use in PV PEC system, the Au nanoparticle electrode was pre-refreshed. Each electrode (1 cm^2) was immersed in the electrolyte, which was K_2CO_3 solution (0.25 M) with saturated CO_2 (pH <7.3). The PV PEC system was performed in a specific gas-tight two-compartment cell (material: acrylic glass; cell window: quartz; individual cell volume: 40 mL; cell boundary diameter: 30 mmφ) made by EC Frontier Co., Inc. Each cell was sealed, and CO_2 (or Ar at type B anolyte) was bubbled through the electrolytes (200 sccm) during the reaction. In the type B condition, CO_2 and Ar were bubbled through the catholyte and anolyte respectively for 1 h before photoirradiation. The cell was irradiated under magnetic stirring (500 rpm) using a solar light simulator (SAN-EI ELECTRIC Corporation, Ltd., Model XES-40S1, 1 SUN: AM 1.5 = 1000 W m^{-2}, Intensity analyzer; KIMO Instruments, Type SL200). During photoirradiation, the current passing through the wire and the applied potential to the Au nanoparticle cathode was measured by a Ag/AgCl reference electrode (sat'd KCl). In addition, the gas-phase and liquid-phase products were analyzed by the same GC and IC systems (mentioned above).

Impedance measurement of the reaction cell: The Nyquist impedance spectra were measured by the following method. The pre-refreshed Au nanoparticle electrode was used as a cathode. A SUS301 plate was used as an anode. The applied potential was −1.0 V (potential amplitude: 10 mV) *vs.* Ag/AgCl (sat'd KCl) and the amplitude was from 0.1 Hz to 1MHz using Ag/AgCl (sat'd KCl) as a reference electrode. Reaction conditions were identical to those in above PV PEC stem for CO production.

2.5. Other analysis

Electrolysis and current measurement for the PV PEC system were measured in an electrochemical analyzer (CH Instruments, Inc., ALS Model 650C). Impedance analysis was performed using a cell test system (Solartron Analytical, 1400 and 1470E). Scanning electron microscope (SEM) observations

were carried out using a Hitachi High-Technologies Corporation SU8020 analytical electron microscope operated at 10 kV. X-ray diffraction (XRD) patterns were measured in a Rigaku Corporation SmartLab. Transmittance spectra were measured with a UV-visible spectrophotometer (Shimazu; UV-2500PC) with bare ITO/Si substrate as a reference. X-ray photoelectron spectroscopy (XPS) measurements were performed using a Physical Electronics, Inc., Quantera-SXM or Quantum-2000 spectrometer using Al Kα radiation as the energy source. Scanning transmission Electron Microscope (STEM) observations were carried out using a Hitachi HD-2700 analytical electron microscope operated at 200 kV, which is equipped with an Energy Dispersive X-ray Spectroscopy (EDS) detector. EDS mapping analysis were taken under STEM mode. XRD, XPS, STEM, and EDS analysis were performed at Toshiba Nanoanalysis Corporation.

3. Results and discussion

3.1. Electrode properties

The anode electrode was composed of a 3jn-a-Si PV cell and a CoO_x catalyst. CoO_x catalysts (thickness: 15 nm) coating the PV surface were prepared by the reactive sputtering method.[11] Fig. 1a shows STEM image of the cross sectional view of CoO_x catalyst, which indicates that the thickness of CoO_x layer is about 15 nm. Moreover, EDS mapping image shows that the element Co exists only the top layer. the XRD pattern of the anode surface, measured at 0.5 degrees incident angle, shows a similar pattern to Co_3O_4 spinel structure (JCPDS 42-1467) (Fig. S1a, ESI†).[12] XPS analysis of the anode shows Co 2p peaks (ca 795.8 and 780.1 eV), which is also similar to Co_3O_4 (Fig. S2a, ESI†).[12,13] The transmittance spectra of CoO_x (thickness: 15 nm) on an ITO/Si electrode, which was synthesized by the reactive same sputtering method as the CoO_x anode on a 3jn-a-Si PV, shows specific absorption bands at about 730 and <500 nm. These bands are derived from ligand-to-metal charge transfer (LMCT) events ($O^{2-} \rightarrow Co^{3+}$ and $O^{2-} \rightarrow Co^{3+}$) and are assigned to Co_3O_4 (Fig. S3, ESI†).[13] These results indicate that the surface CoO_x may be mainly composed of Co_3O_4.

In contrast, the cathode electrode is composed of Au nanoparticles, which were prepared by the pulse-oxidation process. Fig. 1b shows typical photo and SEM images of the Au nanoparticle electrode. Multiple spherical surfaces were observed, and the particle sizes were about 20–50 nm. XRD pattern of the cathode surface, measured at 1.0 degrees incident angle, indicates almost face-centered cubic (FCC) structures of gold metal (JCPDS 04-0784) (Fig. S1b, ESI†).[10] Moreover, XPS analysis of the cathode shows Au 4f peaks (ca 84.0 and 87.6 eV), the valence of which is almost zero (Fig. S2b, ESI†).[9] The cathode surface therefore is composed of metallic Au nanoparticles.

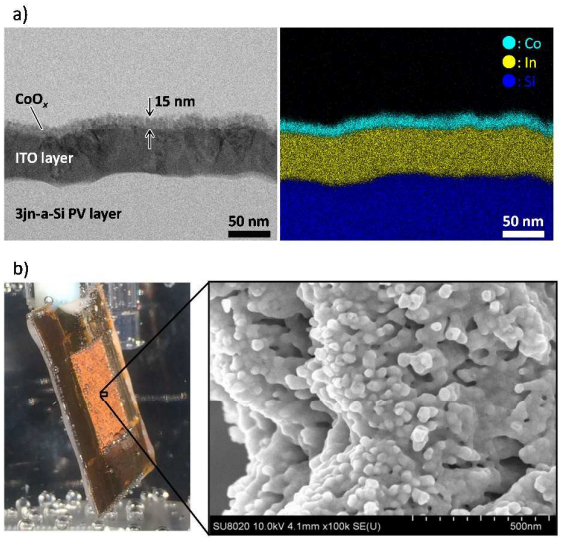

Fig. 1 a) Typical cross-sectional STEM and EDS mapping (cyan: Co, yellow: In, and blue: Si) images and b) Typical photo and SEM images of a Au nanoparticle cathode.

3.2. Electrochemical activity of cathode

The activity of a Au nanoparticle cathode was studied by potentiostatic electrolysis measurement (see experimental section). Fig. 2 shows (a) the partial current density and (b) the faraday efficiency of the reduction products (CO, H_2) on a Au nanoparticle cathode at various applied potentials *vs.* RHE. When the applied potential was <−0.35 V, the faraday efficiency of CO (FE_{CO}) was >97%, and only a small amount of H_2 was generated. Moreover, liquid-phase products such as formic acid and formate species were scarcely detected at all applied potentials (<1 ppb).

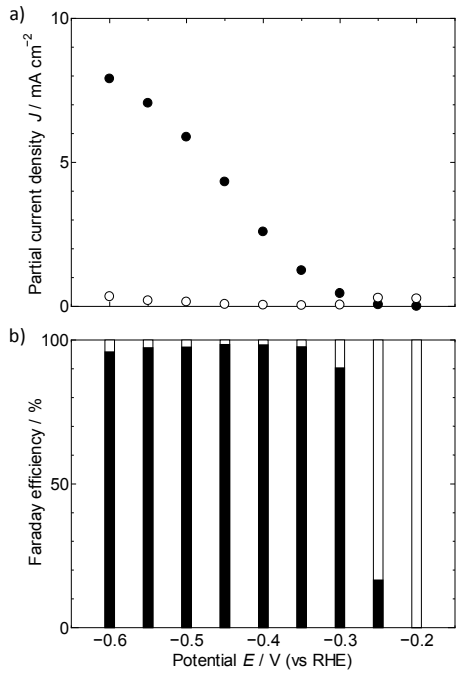

Fig. 2 (a) Partial current density and (b) Faraday efficiency for reduction products on the cathode Au nanoparticle electrode at various potentials. (● and ■) CO and (○ and □) H_2. Amounts of formic acid and formate species were less than detection limit (<1 ppb).

3.3. PV PEC activity for CO production

The activity of the wired PV PEC system for CO production was investigated in a two-compartment cell (each cell volume: 40 mL) of 0.25 M K_2CO_3 solution saturated with CO_2 (pH <7.3) using a SELEMION™ anion exchange membrane. Fig. 3 shows the time-dependent changes in (a) the solar-to-CO conversion efficiency (η_{CO}),[14-16] (b) the operating current density (J), and (c) the FE_{CO} during irradiation of simulated solar light (1 SUN: AM 1.5 = 1000 W m^{-2}). When CO_2 and Ar were used as the bubbling carrier gas through the cathode and anode respectively (type A),[17] the η_{CO} remained approximately 2.0% for 2 h. Moreover, J and FE_{CO} also retained high values (ca. 1.5 mA cm^{-2} and >95%, respectively). In contrast, when CO_2 was used as the bubbling carrier gas through both the anode and cathode during irradiation (type B), the η_{CO} was less than 1.3%. This is because in the type A condition the liquid junction potential is generated by the pH difference (ΔpH) between the catholyte (pH <7.3) and anolyte (pH 9.2), which decreases the overpotentials and increases the η_{CO}. If the liquid junction potential is deducted from η_{CO}, the calculated solar-to-CO conversion efficiency ($\eta_{CO\text{-}cal}$) decrease to approximately 1.9% and is rarely different from η_{CO}.

Liquid junction potential generally decreases with time due to the mixing of an anolyte and a catholyte, leading to decrease of η_{CO}. However, in the type A condition, the liquid junction potential is continuously constant during the reaction. This is because, while the major compositions are different between carbonate (anolyte) and bicarbonate (catholyte) due to different gas bubbling (Ar and CO_2), these species are in equilibrium. No deactivation of η_{CO} due to the mixing electrolytes therefore occurs in the type A condition.

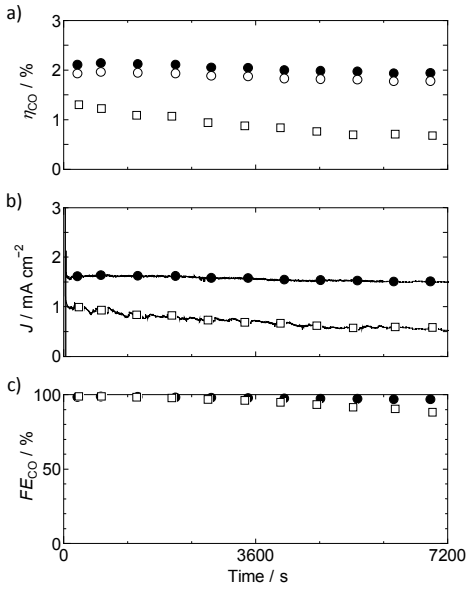

Fig. 3 Time-dependent changes in a) the solar-to-CO conversion efficiency, b) the operating current density, and c) the faraday efficiency of CO and the applied potential at the cathode. Reaction conditions: cathode (Au nanoparticle electrode, 1 cm^2), anode (3jn-a-Si PV cell coated with CoO_x (15 nm), 1 cm^2), anion exchange membrane (SELEMION™), light intensity (1 SUN: AM 1.5 = 1000 W m^{-2}), electrolyte ((type A, ●) cathode: K_2CO_3 solution (0.25 M) with saturated CO_2 in advance, pH 7.3), CO_2 carrier gas, anode: K_2CO_3 solution (0.25 M) with saturated CO_2 in advance and subsequent Ar flow for 1 h, pH 9.2),Ar carrier gas, (type B, □) cathode and anode: K_2CO_3 solution (0.25 M) with saturated CO_2 in advance, pH 7.3), carrier gas CO_2). (○) The $\eta_{CO\text{-}cal}$ at type A.

3.4. Proposed mechanism of CO production by PV PEC system

The PV PEC system for CO production on the wired PV cell with CoO_x and Au nanoparticle electrodes may be realized via the following mechanism: the reaction is initialized by the photoexcitation of a PV cell under solar light irradiation. The excited PV cell produces electron (e^-) and positive hole (h^+) pairs.

$$PV + h\nu \rightarrow h^+ + e^-$$

The e^- transfers to cathode Au nanoparticles and reduces CO_2 to a $CO_2\bullet^-$ intermediate. Then, protonation of $CO_2\bullet^-$ by HCO_3^- produces a $HCO_2\bullet$ radical.[9] Subsequently, a $HCO_2\bullet$ is probably reduced by the e^- and protonated by HCO_3^- again, leading to production of CO, CO_3^{2-}, and H_2O. CO_3^{2-}, which is obtained as a by-product, readily reacts with H_2O to produce HCO_3^- and OH^-.

$$CO_2 + e^- \rightarrow CO_2\bullet^-$$

$$CO_2\bullet^- + HCO_3^- \rightarrow HCO_2\bullet + CO_3^{2-}$$

$$HCO_2\bullet + e^- + HCO_3^- \rightarrow CO + CO_3^{2-} + H_2O$$

$$2CO_3^{2-} + 2H_2O \rightarrow 2HCO_3^- + 2OH^-$$

Therefore, the total cathode reaction is as follows:

$$CO_2 + H_2O + 2e^- \rightarrow CO + 2OH^-$$

In contrast, the h^+ transfers to the anode CoO_x catalysts and oxidizes OH^- to produce oxygen (O_2) and H_2O.

$$2OH^- + 2h^+ \rightarrow 1/2O_2 + H_2O$$

The total reaction is therefore shown as CO_2 decomposition to CO and O_2, as follows:

$$CO_2 \rightarrow CO + 1/2O_2$$

In this reaction, HCO_3^- and CO_3^{2-} in the electrolyte also have the potential to become a carbon source. This is because the dissolved CO_2 is in equilibrium with HCO_3^- and CO_3^{2-}.[18]

3.5. Theoretical estimation of solar-to-CO conversion efficiency

These solar-to-CO conversion efficiencies are significantly affected by the liquid junction potential generated by the pH difference between anolyte and catholyte. This can be clarified by a theoretical estimation based on the electrochemical properties of electrodes and PV cells (for a detailed explanation, see ESI†).[19] The electrochemical properties of electrodes are obtained from summation of the

partial electrochemical activities of the anode and cathode. For proceeding electrochemical oxidation of H_2O (+1.23 V vs. RHE) and reduction of CO_2 (−0.10 V vs. RHE), 1.33 V is theoretically necessary. However, the actual operating voltage in the reaction (*V*) was larger than 1.33 V due to the presence of overpotentials, which were mainly categorized as (i) reaction overpotential (ΔV_{react}), (ii) concentration overpotential (ΔV_{conc}), or (iii) resistance overpotential (ΔV_{resist}). The reaction activity of the electrodes is therefore estimated by the following equation:

$$V = 1.33 + \Delta V_{react} + \Delta V_{conc} + \Delta V_{resist}$$

In addition, when the pH is different between an anolyte and a catholyte, the liquid junction potential (ΔV_{pH}) is generated and acts as chemical bias. The value of ΔV_{pH} must be deducted from *V* in the calculated equation. Therefore, the reaction activity is exhibited by the following equation:

$$V = 1.33 + \Delta V_{react} + \Delta V_{conc} + \Delta V_{resist} - \Delta V_{pH} \quad (1)$$

In contrast, the PV cell property can be estimated from the current-voltage curve of the PV. The current-voltage curve of the PV cell is therefore exhibited by the following equation:

$$J = J_{ph} - J_d$$

J, J_{ph} and J_d are respectively the operating current density, the photocurrent density and dark current density. However, the PV cell surface is coated with the CoO_x anode catalyst. The current-voltage curve therefore deceases due to its transmittance (T_{sum}). The actual specific curve of the PV cell is thus given by the following equation.

$$J = T_{sum} J_{ph} - J_d \quad (2)$$

The *J* is therefore the point of intersection between Eqn (1) and (2). Moreover, the partial current density of CO generation decreases the ratio of FE_{CO}. Therefore, the partial current density of CO generation (J_{CO}) is obtained by the following equation:

$$J_{CO} = J \cdot FE_{CO}$$

Thus, the solar-to-CO conversion efficiency is exhibited by the following equation:[14]

$$\eta_{CO}\,[\%] = \frac{1.33\,[\mathrm{V}] \cdot J_{CO}}{P \cdot A} \cdot 100 = \frac{S_{CO}\,[\mathrm{W\ m^{-2}}]}{P \cdot A} \cdot 100$$

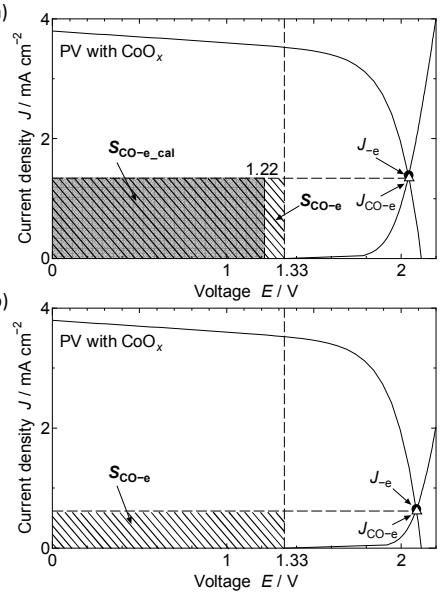

Fig. 4 Current density *vs.* voltage curves of the estimated results for wired PV PEC systems for type A and B. J_{-e} is the *estimated* operating current density.

The value of the effective power density for CO generation (S_{CO}) directly affects the conversion efficiency of CO generation. Fig. 4 shows simulation results of the PV cell and electrode activity curves (Table S1, ESI†). Fig. 4a shows the result for type A. In this case, the *estimated* partial current density of CO ($J_{CO\text{-}e}$) is 1.4 mA cm^{-2}. The *estimated* solar-to-CO conversion efficiency ($\eta_{CO\text{-}e}$) is 1.8% (FE_{CO} = 97%). These values are slightly smaller than the experimental results (Fig. 3a), because the anode CoO_x activity on an ITO/Si electrode is estimated to be lower than that on a PV cell due to the ITO/Si electrode surface being smoother than the PV cell surface. In addition, if the liquid junction potential (ΔpH = 1.9, ΔV_{pH} = ca. 112 mV) is deducted, the *estimated* power density for CO generation ($S_{CO\text{-}e}$, shaded area) decreases to the *estimated* and calculated solar-to-CO conversion efficiency ($S_{CO\text{-}e\_cal}$, darker shaded area), and the *estimated* and calculated solar-ro-CO conversion efficiency ($\eta_{CO\text{-}e\_cal}$) slightly decreases to 1.7%. In addition, the theoretical maximum efficiency of solar-to-CO conversion $\eta_{CO\text{-}e\_max}$ is estimated at 1.9% when all conditions are same with the exception of electrolyte. In this PV PEC system, the anolyte is composed of potassium carbonate solution (0.25 M) with CO_2 bubbling in advance (pH <7.3). When Ar bubbling is performed on the anolyte solution, the value of pH is shifted from <7.3 to 9.5 unless the anolyte is heated. Therefore the theoretical maximum pH difference $\Delta pH_{\_max}$, the theoretical maximum liquid junction potential ΔV_{pH_max}, and the theoretical maximum partial current density of CO generation $J_{CO\text{-}e\_max}$ are respectively estimated at 2.2, 130 mV, and 1.5 mA cm^{-2}. However, in reality the bicarbonate anion species in the catholyte (pH <7.3) flow into the anolyte through the membrane, and the pH value of anolyte is stabilized at 9.2. This indicates that the $\eta_{CO\text{-}e}$ (1.8%) is obtained by the use of the maximum liquid junction potential possible.

In contrast, in the type B condition (CO_2 bubbling in both electrolytes), $J_{CO\text{-}e}$ (0.64 mA cm^{-2}) and $\eta_{CO\text{-}e}$ (0.82%) significantly decrease because ΔV_{pH} is zero which leads to no decrease in the total overpotentials (Fig. 4b). Comparing $\eta_{CO\text{-}e}$ in type B with $\eta_{CO\text{-}e\_cal}$ in type A under the same condition without ΔV_{pH}, $\eta_{CO\text{-}e\_cal}$ in type A is approximately twice larger than $\eta_{CO\text{-}e}$ in type B. These results indicate that ΔV_{pH} expands the capability of PV PEC system, and plays a crucial role in generating the high η_{CO} value. Meanwhile, when the electrode activities are high enough and J is close to short-circuit current density J_{SC} of PV cells, the J_{CO} and the η_{CO} will scarcely increase by the effect of ΔV_{pH}. Therefore, the adaptation to the condition that the J_{tot} is much lower than J_{SC} is necessary in order to make the best use of ΔV_{pH} for enhancement of the η_{CO}.

4. Conclusion

We found that the wired 3jn-a-Si PV PEC system with CoO_x and Au nanoparticle electrodes in different carbonate electrolytes promotes efficient solar-to-CO conversion (η_{CO} ≥2.0%) from CO_2 and H_2O under solar light irradiation. The efficiency of this PV PEC system is sustainable for 2 h due to the contribution of the electrolytes which generate sustainable ΔV_{pH}, in addition to the combination of the 3jn-a-Si PV cell with wide visible light absorption range with the electrodes with low overpotentials and high selectivity of CO_2 reduction. The estimated conversion efficiencies based on the electrochemical properties of the PV cell and the electrodes exhibit that ΔV_{pH} plays a crucial role for η_{CO}. The solar fuel system using the PV PEC system presented here may contribute to the design of more sustainable artificial photosynthesis systems for developing solutions to global warming and fuel problems.

Notes and references

1 (*a*) M. R. Wasielewski, *Chem. Rev.,* 1992, **92**, 435-461; (*b*) A. J. Bard and M. A. Fox, *Acc. Chem. Res.,* 1995, **28**, 141-145; (*c*) T. J. Meyer, *Acc. Che. Res.,* 1989, **22**, 163-170; (*d*) D. Gust, T. A. Moore and A. L. Moore, *Acc. Chem. Res.,* 2009, **42**, 1890-1898; (*e*) B. Kasemo, *Surf. Sci.,* 2002, **500**, 656-677.

2 (*a*) B. O'Regan and M. Grätzel, *Nature*, 1991, **353**, 737-740; (*b*) M. Law, L. E. Greene, J. C. Johnson, R. Saykally and P. Yang, *Nat. Mater.,* 2005, **4**, 455-459; (*c*) A. Hagfeldt and M.Grätzel, *Acc. Chem. Soc.,* 2000, **33**, 269-277; (*d*) G. McDermott, S. M. Prince, A. A. Freer, A. M. Hawthornthwaite-Lawless, M. Z. Papiz, R. J. Cogdell and N. W. Isaacs, *Nature*, 1995, **374**, 517-521.

3 (*a*) A. Fujishima and K. Honda, *Nature*, 1972, **238**, 37-38; (*b*) S. U. M. Khan, M. Al-Shahry and W. B. Ingler Jr., *Science*, 2002, **297**, 2243-2245; (*c*) A. Kudo and Y. Miseki, *Chem. Soc. Rev.,* 2009, **38**, 253-278; (*d*) X. Chen, S. Shen, L. Guo and S. S. Mao, *Chem. Rev.,* 2010, **110**, 6503-6570; (*e*) Z. Zou, J. Ye, K. Sayama and H. Arakawa, *Nature*, 2001, **414**, 625-627; (*f*) M. G. Walter, E. L. Warren, J. R. McKone, S. W. Boettcher, Q. M. Elizabeth, A. Santori and N. S. Lewis, *Chem. Rev.,* 2010, **110**, 6446-6473; (*g*) M. W. Kanan and D. G. Nocera, *Science*, 2008, **321**, 1072-1075; (*h*) K. Maeda, K. Teramura, D. Lu, T. Takata, N. Saito, Y. Inoue and K. Domen, *Nature,* 2006, **440**, 295.

4 (*a*) X. Wang, K. Maeda, A. Thomas, K. Takanabe, G. Xin, J. M. Carsson, K. Domen and M. Antonietti, *Nat. Mater.,* 2009, **8**, 76-80; (*b*) M. Ni, M. K. H. Leung, D. Y. C. Leung and K. Sumathy, *Renewable Sustainable Energy Rev.,* 2007, **11**, 401-425; (*c*) D. Das and T. N. Veziroğlu, *Int. J. Hydrogen Energy,* 2001, **26**, 13-28; (*d*) O. Khaselev and J. A. Turner, *Science*, 1998, **280**, 425-427; (*e*) Q. Li, B. Guo, J. Yu, J. Ran, B. Zhang, H. Yan and J. R. Gong, *J. Am. Chem. Soc.,* 2011, **133**, 10878-10884.

5 (*a*) T. Inoue, A. Fujishima. S. Konishi and K. Honda, *Nature*, 1979, **277**, 637-638; (*b*) S. C. Roy, O. K. Varghese, M. Paulose and C. A. Grimes, *ACS Nano*, 2010, **4**, 1259-1278; (*c*) W. Leitner, *Angew. Chem. Int. Ed.,* 1995, **34**, 2207-2221; (*d*) E. E. Benson, C. P. Kubiak, A. J. Sathrum and J. M. Smieja, *Chem. Soc. Rev.,* 2009, **38**, 89-99; (*e*) H. Takeda, K. Koike, H. Inoue and O. Ishitani, *J. Am. Chem. Soc.,* 2008, **130**, 2023-2031; (*f*) Y. Hori, in *Modern Aspects of Electrochemistry, e*d. C. G. Vayenas, R. E. White and M. E. Gamboa-Aldeco, Springer, New York, 2008, vol. 42, pp. 89-189.

6 (*a*) M. Halmann, M. Ulman and B. Aurian-Blajeni, *Sol. Energy,* 1983, **31**, 429-431; (*b*) O. K. Varghese, M. Paulose, T. J. LaTempa and C. A. Grimes, *Nano Lett.,* 2009, **9**, 731-737; (*c*) K. Iizuka, T. Wato, Y. Miseki, K. Saito and A. Kudo, *J. Am. Chem. Soc.,* 2011, **133**, 20863-20868; (*d*) S. Sato, T. Arai, T. Morikawa, K. Uemura, T. M. Suzuki, H. Tanaka and T. Kajino, *J. Am. Chem. Soc.,* 2011, **133**, 645-648; (*e*) T. Arai, S. Sato, T. Kajino and T. Morikawa, *Energy Environ. Sci.,* 2013, **6**, 1274-1282; (*f*) S. Yotsuhashi, M. Deguchi, Y. Yamada and K. Ohkawa, *AIP Adv.,* 2014, **4**, 067135-1-067135-8; (*g*) J. L. White, J. T. Herb, J. J. Kaczur, P. W. Majsztrik and A. B. Bocarsly, *J. CO_2 Util.,* 2014, **7**, 1-5; (*h*) H. S. Jeon, J. H. Koh, S. J. Park, M. S. Jee, D.-H. Ko, Y. J. Hwang and B. K. Min, *J. Mater. Chem. A,* 2015, **3**, 5835-5842.

7 S. Y. Reece, J. A. Hamel, K. Sung, T. D. Jarvi, A. J. Esswein, J. J. H. Pijpers and D. G. Nocera, *Science*, 2011, **334**, 645-648.

8 (*a*) J. O. M. Bockris and J. C. Wass, *J. Electrochem. Soc.,* 1989, **136**, 2521-2528; (*b*) K. Chandrasekaran and L. O. M. Bockris, *Surf. Sci.,* 1987, **185**, 495-514.

9 Y. Chen, C. W. Li and M. W. Kanan, *J. Am. Chem. Soc.,* 2012, **134**, 19969-19972.

10 Y. Chen, C. Somsen, S. Milenkovic and A. W. Hassel, *J. Mater. Chem.,* 2009, **19**, 924-927.

11 (*a*) W. Estrada, M. C. A. Fantini, S. C. De Castro, C. N. Pole da Fonseca and A. Gorenstein, *J. Appl. Phys.,* 1993, **74**, 5835; (*b*) W. B. Ingler Jr., D. Attygalle and X. Deng, *ECS Trans.,* 2006, **3**, 261-266.

12 X. Wang, X. Chen, L. Gao, H. Zheng, Z. Zhang and Y. Qian, *J. Phys. Chem. B,* 2004, **108**, 16401-16404.

13 D. Barreca and C. Massignan, *Chem. Mater.,* 2001, **13**, 588-593.

14 The solar-to-CO conversion efficiency η_{CO} was calculated as follows:(ref. 15)

$$\eta_{CO}\,[\%] = \frac{R_{CO}\cdot \Delta G^{0}_{CO}}{P\cdot A}\cdot 100 = \frac{1.33\,[\mathrm{V}]\cdot J_{CO}}{P\cdot A}\cdot 100$$

R_{CO}, $\Delta G_{CO}{}^{0}$, *P, A and* J_{CO} are respectively the rate of CO production (mol s^{-1}), the change in the Gibbs free energy (257.2 kJ mol^{-1}, (ref 16)), irradiation light intensity (1 kW m^{-2}), acceptance surface area of the PV cell (1 cm^2) and the partial current density of CO generation.

15 Q. Wang, T. Hisatomi, S. S. K. Ma, Y. Li and K. Domen, *Chem. Mater.,* 2014, **26**, 4144-4150.

16 J. A. Herron, J. Kim, A. A. Upadhye, G. W. Huber and C. T. Maravelias, *Energy Environ. Sci.,* 2015, **8**, 126-157.

17 Ar pre-bubbling in the anolyte is performed for 1h before the reaction, and the pH of anolyte changes from <7.3 to 9.2 by CO_2 degassing.

18 H. Zhong, K. Fujii, Y. Nakano and F.Jin, *J. Phys. Chem. C,* 2015, **119**, 55-61.

19 (*a*) A. J. Bard and L. R. Faulkner, in *Electrochemical methods: fundamentals and applications,* ed. D. Harris, E. Swain, C.

Robey and E. Aiello, John Wiley & Sons Inc., New York, 2nd edn., 2001, pp. 63-74, pp. 87-136 and pp. 368-388; (*b*) Y. Matsuda and C. Iwakura, in *Denkikagakugairon, 1st ed.* (Eds. J. Shiokawa, H. Matsuda, Y. Matsuda, H. Taniguchi), Maruzen, Tokyo, 1994, pp. 51-71.